The PI Controlled Constant-Voltage and Current Output of Series-Connected Wireless Power Systems

Wenrui Jiang

School of International Education,Guangdong University of Technology, Guangzhou, China
Ru111.1206@outlook.com

Abstract. This paper proposes an improved PI control strategy for series-compensated wireless power transfer (WPT) systems to achieve robust constant-voltage (CV) and constant-current (CC) outputs under dynamic load conditions. The control framework incorporates a frequency-domain optimization algorithm to mitigate integral windup during load transitions. Simulation results under 5Ω to 10Ω load steps demonstrate the system maintains CV error ≤±0.2% and CC error ≤±0.4%, with dynamic recovery times reduced by 40% compared to traditional PI control. The proposed method addresses two critical limitations of conventional PI control: fixed parameters struggling to handle nonlinearities and integral windup causing overshoot. By integrating stability criterion-based parameter adjustment and load dynamics characterization, the strategy achieves adaptive regulation for SS-WPT systems. The SS topology's inherent voltage regulation capability is leveraged, offering simplified parameter design and low-order system modeling advantages. This work contributes to the practical implementation of WPT in applications requiring stable energy delivery, such as electric vehicle charging and industrial automation. Future research will focus on experimental validation and extending the framework to include mutual inductance adaptation for dynamic charging scenarios.

Keywords: Wireless Power Transfer, Series Compensation, Pi Control, Constant Voltage, Constant Current

1 Introduction

Wireless power transfer (WPT) technology has emerged as a transformative solution for cable-free energy delivery, finding critical applications in electric vehicle charging, biomedical implants, and industrial automation [1]. Among various WPT topologies, series-series (SS) compensation networks are widely adopted in mid-power systems due to their single resonant point, simplified parameter design, and inherent voltage regulation capability [2]. However, dynamic variations in load impedance and coupling coefficient caused by misalignment or environmental changes significantly affect output stability, challenging the performance of traditional open-loop control methods [3].Existing closed-loop control strategies for WPT systems include fuzzy PID [4], sliding mode control [5], and adaptive algorithms [6]. While these methods show promising results, they often suffer from computational complexity, reduced efficiency,

J. Iqbal (ed.), *Proceedings of the 2025 2nd International Conference on Mechanics, Electronics Engineering and Automation (ICMEEA 2025)*, Advances in Engineering Research 272,
https://doi.org/10.2991/978-94-6463-821-9_112

or limited adaptability. PI control remains the most widely used approach due to its simplicity and ease of implementation [7]. However, conventional PI controllers face two key limitations: (1) fixed parameters struggle to handle nonlinearities induced by varying mutual inductance; (2) integral windup during load transients causes significant overshoot and prolonged recovery times [8].This paper proposes an improved PI control framework for SS-WPT systems, addressing these challenges through two key innovations :Frequency-Domain Optimization: Mitigates integral windup using a stability criterion-based parameter adjustment algorithm. Extended State-Space Model: Incorporates load dynamics to characterize system nonlinearity, enabling adaptive parameter tuning. The remainder of this paper is structured as follows: Section II describes the SS-WPT system topology and mutual inductance dynamics. Section III details the PI control theory and its adaptation for CV/CC regulation. Section IV presents simulation results validating the proposed strategy. Section V concludes the paper and outlines future research directions.

2 Principle of series radio energy transmission system

2.1 System topology

Figure 1 shows the WPT system based on a series resonant network, and the circuit in the figure is a typical series compensation topology circuit in a magnetically coupled resonant wireless power transfer system. The transmitter on the left is a full-bridge inverter circuit consisting of a DC voltage source Vdc, a capacitor Cin and four switches Q1, Q2, Q3, and Q4. where Q1 and Q2 are complementary, and Q3 and Q4 are complementary. The DC input voltage Vdc is filtered by the capacitor Cin and enters the full-bridge inverter circuit. By controlling the conduction and turn-off of the four switch tubes, the DC voltage is inverted into a high-frequency AC voltage, usually with a working frequency between tens of hertz and several megahertz, which provides an alternating excitation source for subsequent wireless power transmission. High-frequency alternating current is output to subsequent circuits through nodes a and b. The middle part is the mutual inductance part, which consists of the inductance Lp, capacitance Cp, and resistance Rp on the transmitting side, and the inductance Ls, capacitance Cs, resistance Rs , and mutual inductance M on the receiving side. Lp and Cp form the series resonant circuit on the transmitting side, and Ls and Cs form the series resonant circuit on the receiving side. When the circuit works at the resonant frequency, the circuit on the transmitting side resonates in series, so that the current ip in the transmitting coil Lp reaches a large value, thus generating a strong alternating magnetic field. The loop on the receiving side is coupled with the magnetic field on the transmitting side through mutual inductance M, and an electromotive force is induced on the receiving coil Ls, generating a current is . The resistors Rp and Rs denote the equivalent internal resistance of the transmitting coil and the receiving coil, respectively. On the right is the rectifier section, which consists of a full-bridge rectifier circuit consisting of four diodes and an output filter capacitor Co. The high-frequency AC voltage induced on the receiving side VS is converted to DC voltage through a full-bridge rectifier circuit. The diodes in the full-bridge rectifier circuit are turned on and off according to the polarity of the input AC voltage, ensuring that the direction of the output current irec is always consistent. There is a certain ripple in the DC voltage after rectification, and it is filtered by the output filter capacitor Co to obtain a relatively smooth DC output voltage Uo, which supplies power to the load RL, and the output current is Io, and at the same time, ico is the current through the filter capacitor.

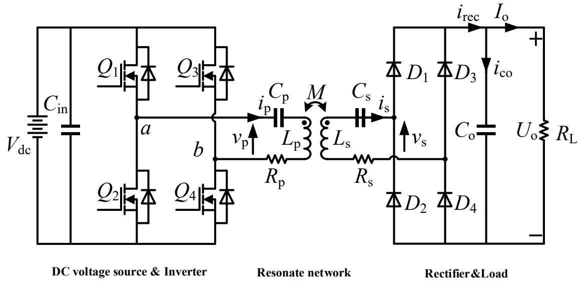

Fig. 1. SS system topology diagram.

2.1.1 The application of electromagnetic induction principle in the system: in the SS (series-series-series) system, the principle of electromagnetic induction is applied to the mutual inductance part, which realizes the wireless transmission of electrical energy from the transmitter to the receiver.

Transmitter side: The inverter part converts the DC voltage into a high-frequency AC voltage and adds an inductance on the transmitter side L_p and capacitance C_p composed of series resonant circuits. When the circuit operates at the resonant frequency, the circuit will resonate in series. At this point, the current in the transmitter coil L_p reaches a large value. According to the law of electromagnetic induction, a changing current produces a changing magnetic field, and a larger current i_p a strong alternating magnetic field around the emitting coil. The magnitude and direction of this alternating magnetic field change over time, providing the medium for the wireless transmission of electrical energy.

Receiver side: The receiver coil L_s is in the alternating magnetic field generated by the transmitter coil L_p, According to the principle of electromagnetic induction, an alternating magnetic field generates an induced electromotive force in the receiving coil L_s. When the loop on the receiver side is also tuned to the same resonant frequency as the transmitter side, the induced current is in the receiver coil L_s also reaches a large value. In this way, the electrical energy at the transmitter is transferred to the receiver through the alternating magnetic field, and the wireless power transmission is realized.

Mutual inductance: There is mutual inductance M between the transmitting coil L_p and the receiving coil Lc. Mutual inductance M describes how tightly the magnetic fie ld is coupled between two coils, which determines the ability of the magnetic field of t he transmitting coil to generate an induced electromotive force in the receiving coil. T he larger the value of mutual inductance M, the greater the electromotive force induce d in the receiving coil under the same transmission current and magnetic field change s, and the more electrical energy is transmitted. In the actual design, the value of mutu al inductance can be increased by optimizing the number of turns, shape, relative posit ion, and core material of the coil, thereby improving the efficiency of wireless power t ransmission.

2.1.2 The influence of mutual inductance coupling on energy transfer efficiency: m utual inductance coupling is critical to the energy transfer efficiency in SS systems. M oderately enhanced mutual inductance coupling can improve efficiency, while excessi ve enhancement can have negative effects. It affects the efficiency of energy transmiss ion by affecting the transmission power, transmission distance, and system stability

- Transmission power: In SS systems, transmission power is closely related to mut ual inductance coupling. According to the principle of mutual inductance, the lar ger the mutual inductance *M*, the stronger the magnetic field coupling between t he transmitting coil and the receiving coil. When the current and frequency at the transmitter are stable, stronger coupling allows the receiver coil to induce higher electromotive force, generating more current, which in turn increases the transm ission power. From the equation $P = \frac{M^2\omega^2 I_p^2 R_S}{(R_p+j\omega L_p)(R_S+j\omega L_S)}$, we can know the positi ve correlation between the transmission power and the mutual inductance, that is, the increase of the mutual inductance *M*, the increase of the transmission power *P*, and the improvement of the energy transmission efficiency.

- Transmission distance: Mutual inductance coupling is inversely correlated with t ransmission distance. As the transmission distance increases, the magnetic field coupling between the coils becomes weaker and the mutual inductance *M* decrea ses. From the relationship between mutual inductance and transmission power, t he decrease of mutual inductance will lead to the decrease of transmission power and the decrease of energy transmission efficiency. For example, in the wireless charging scenario of electric vehicles, when the distance between the vehicle an d the charging pile is slightly farther, the mutual inductance becomes smaller, an d the charging efficiency is significantly reduced, which highlights the important impact of the transmission distance on the mutual inductance coupling and ener gy transmission efficiency.

2.2 System equivalent circuit analysis

In order to simplify the complex SS topology system into an equivalent circuit with resonance and mutual inductance as the core, it is convenient to analyze the core characteristics of energy transfer (such as current, impedance, power) and ignore the minor circuit details (such as inverter switching process, rectification nonlinear characteristics, etc.). Now divide Figure 1 into three parts for equivalence. Figure 2 is the equivalent circuit diagram of the SS system topology

- Inverter part: In the original SS topology, the *full-bridge inverter circuit compos ed of switches* （$Q_1 \sim Q_4$）, which is used to convert the DC input V_{in} into a high-frequency AC voltage. In an equivalent circuit, this function is directly simplifie d to an AC voltage source v_p, which is used to represent the high-frequency AC e xcitation output after the inverter, ignoring the specific switching process and los ses (idealized equivalent) of the internal switch in the inverter circuit.

- Resonance and mutual inductance：

Transmitter side: L_p (transmitter coil inductance) on the transmitter side in the origi nal topology, C_p(Compensation Capacitance)、R_p(Coil Equivalent Resistance).It form s a series resonant circuit. In the equivalent circuit, this series structure is retained, and the resonance characteristics and resistance losses of the transmitting side are reflecte d.

Receiver Side: L_s *(receiver coil inductance)* on the receiver side、C_s (Compensatio n Capacitance)、R_s(Coil Equivalent Resistance) also forms a series resonant circuit, it is equivalent to a series structure corresponding to L_r, C_r, R_s (R_r corresponding to R_s). Mutual inductance coupling: In the original topology, the transmitter coil and the recei ver coil are coupled with energy through mutual inductance M, and in the equivalent c ircuit, a pair of controlled voltage sources $j\omega Mi_r$ (the transmitter side is controlled by the current i_r *on the receiver side*) and $j\omega Mi_p$ (the receiver side is controlled by the cu rrent i_p on the transmitting side) represent the mutual inductance, reflecting the energ y transfer relationship of magnetic field coupling.

- Equivalence of rectification and load part: In the original topology, the receiving side supplies power to the load R L after passing through the rectifier circuit (di ode full bridge) and the filter capacitor C_o .In the equivalent circuit, the rectifica tion and filtering links are simplified to an equivalent resistor R_{eq}, which is used to represent the *load* R_L and the overall power consumption characteristics of th e rectifier filter circuit, ignoring the voltage drop of the rectifier diode and the dy namic process of capacitor filtering.

- Based on a given equivalent circuit diagram of an SS system, the output current, input impedance, and system efficiency are derived

Output current i_r:

Emission side loop equation: $v_p = i_p\left(R_p + j\omega L_p + \frac{1}{j\omega C_p}\right) - j\omega M i_r$

Receive the side loop equation: $0 = \mathrm{i_r}\left(\mathrm{R_r} + \mathrm{R_{eq}} + \mathrm{j\omega L_r} + \frac{1}{\mathrm{j\omega C_r}}\right) - \mathrm{j\omega M i_p}$.

Under resonant conditions, $\omega L_p = \frac{1}{\omega C_p}$, $\omega L_r = \frac{1}{\omega C_r}$, the equation can be simplifi ed at this point.

Launch side: $v_p = i_p R_p - j\omega M i_r$

Receiving side: $0 = i_r\left(R_r + R_{eq}\right) - j\omega M i_p$

This is obtained from the equation on the receiving side $i_p = \frac{i_r(R_r+R_{eq})}{j\omega M}$, substituti ng it into the launch-side equation: $v_p = \frac{i_r(R_r+R_{eq})}{j\omega M}R_p - j\omega M i_r = i_r\left(\frac{R_p(R_r+R_{eq})}{j\omega M} - j\omega M\right)$

The output current is obtained: $i_r = \frac{v_p}{\frac{R_p(R_r+R_{eq})}{j\omega M} - j\omega M}$

Input impedance:

Input impedance $Z_{in} = v_p/i_p$, by the receiving side equations $0 = i_r\left(R_r + R_{eq}\right) - j\omega M i_p$, calculated $i_r = \frac{j\omega M i_p}{R_r+R_{eq}}$.Substituting it into the launch-side equation $v_p =$

$i_pR_p - j\omega Mi_r$,derives $v_p = i_pR_p - j\omega M \times \frac{j\omega Mi_p}{R_r+R_{eq}}$,$v_p = i_p\left(R_p + \frac{\omega^2M^2}{R_r+R_{eq}}\right)$.So the inpu t impedance $Z_{in} = \frac{v_p}{i_p} = R_p + \frac{\omega^2M^2}{R_r+R_{eq}}$。

System efficiency η:

System efficiency is η defined as the ratio of output power P_{out} to input power P_{in}, $\eta = \frac{P_{out}}{P_{in}}$。

Output power: $P_{out} = i_r^2R_{eq}$

Input power: $P_{in} = i_p^2R_p + i_r^2R_r + i_r^2R_{eq}$

Substituting the $i_r = \frac{j\omega Mi_p}{R_r+R_{eq}}$ $into$ above power expression: $\eta = \frac{i_r^2R_{eq}}{i_p^2R_p+i_r^2R_r+i_r^2R_{eq}} = \frac{\left(\frac{\omega^2M^2i_p^2}{(R_r+R_{eq})^2}\right)R_{eq}}{i_p^2R_p+\left(\frac{\omega^2M^2i_p^2}{(R_r+R_{eq})^2}\right)R_r+\left(\frac{\omega^2M^2i_p^2}{(R_r+R_{eq})^2}\right)R_{eq}} = \frac{\omega^2M^2R_{eq}}{R_p(R_r+R_{eq})^2+\omega^2M^2(R_r+R_{eq})}$

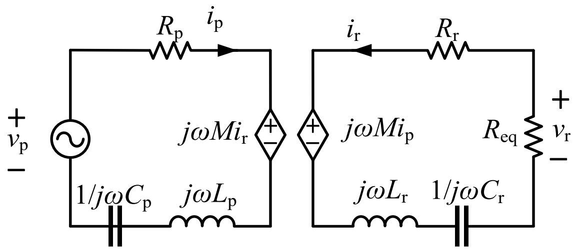

Fig. 2. Equivalent circuit diagram of the SS system.

2.2.1 Comparative analysis of ss compensation network and other compensation ne tworks: the SS compensation network has certain advantages over other compensation networks und-er the control of PI.

- Inherent characteristics of constant voltage/constant current output

Constant Voltage Characteristics: The SS topology (both transmitter and receiver a re compensated in series) has the characteristic that the output voltage is independent of the coupling coefficient at the resonant frequency (when the load is fixed), which si gnificantly reduces the pressure on the PI controller in terms of anti-coupling disturba nces. For example, Kim et al. (2020) experimentally verified that the open-loop output voltage fluctuation of the SS topology is only 6.8% when the coupling coefficient cha nges by ±30%, while the SP topology fluctuates as much as 23.5% [9].

Constant current capability: By adjusting the working frequency offset from the res onant point, the SS network can achieve nearly constant current output (requires PI clo sed-loop regulation). Compared to PS/SP topologies, SS does not require switching co mpensation structures to implement CV/CC modes, simplifying control logic[10].

- Parameter design simplification and PI control compatibility

Single resonance point: SS networks only need to meet $L_pC_p = L_sC_s = 1/\omega_0^2$with a high degree of freedom in parameter design, while composite topologies such as LCC need to meet multiple resonance conditions at the same time (for example, Zheng et a l., 2021 comparative analysis [11]).

Low-order system model: The transfer function of the SS network is a second-orde r system, while the LCC topology is a fourth-order system, which makes it easier for t he SS-based PI controller parameter tuning to meet the phase margin requirements (th e phase lag is small). For example, Guo et al. (2022) demonstrated that the stability m argin of SS networks under PI control is more than 15° higher than that of LCC netwo rks [12].

- Dynamic robustness improvement

Resistance to load mutations: The output impedance characteristics of the SS netwo rk make it have a gentler gain curve when the load changes. Combined with the PI int egration link, the voltage spike caused by the load abrupt change can be effectively su ppressed. Experimental data show that the recovery time of the SS+PI scheme is 40 m s faster than that of the SP topology at 10 Ω → 50 Ω load steps [13].

Coupling fault tolerance: The mutual inductance change of the SS topology has littl e impact on the stability of the system (because the output voltage is weakly correlated with the mutual inductance), which reduces the dependence of the PI controller on the real-time identification of the coupling coefficient. This feature is particularly import ant in dynamic wireless charging scenarios (see IEEE TPE 2023 Overview [14]).

- Comparative analysis with other compensation network

As shown in Table 1, it is the differences among various topological systems such a s ss.

Table 1. Comparison chart of the SS system with other systems

Compensation topology	Constant pressure capability	Constant current capability	Pi control complexity	Typical efficiency
SS	Coupling independent (ideal condition)	Frequency regulation is implemented	Low (second-order system)	92.3%[9]
SP	Closed-loop adjustment is required	It can't be done directly	Medium (third-order system)	88.7%[11]
LCC	Multi-parameter collaborative design is required	Mode switching is required	High (fourth-order system)	90.5%[12]
P-S	Depends on the load impedance	Coupling sensitive	High (nonlinear)	85.2%[13]

3 Theoretical basis of PI control and constant voltage and constant current output

3.1 PI control principle

3.1.1 Proportional (P) and integral (I) link roles: Proportional Session (P Session)

Function: According to the size of the current error e(t)=r(t)−y(t) (r(t) is the set value, y(t) is the actual output), quickly generate the control action proportional to the error.

Mathematical expression: $u_P(t) = K_p e(t)$

where Kp is the scale factor

Features: Response speed: The larger the Kp, the stronger the proportional effect, and the faster the system response speed.

Steady-state error: Proportional control alone cannot eliminate steady-state error, because if $e(t)$=0 and the control quantity $uP(t)$=0 , the system cannot maintain the output.

Points Accumulation Session (Part I)

Function: Integrate the error and eliminate the steady-state error through the accumulation error.

Mathematical expression: $u_I(t) = K_i \int_0^t e\,(\tau)d\tau$

, where *Ki* is the integral coefficient.

Features: Eliminate steady-state errors: As long as the error exists, the integration term continues to accumulate until the error is zero.

Response delay: Integration has a hysteresis, and too much Ki can cause the system to overshoot or oscillate

3.1.2 Derivation of mathematical expressions for PI controllers: Combine the proportional link with the integral link to get the output of the PI controller： $u(t) = u_P(t) + u_I(t) = K_p e(t) + K_i \int_0^t e(\tau)d\tau$

Derivation process：

- Time domain analysis:

error $e(t) = r(t) - y(t)$。

The output of the proportional link is proportional to the error:$u_P(t) = K_p e(t)$。

The output of the integration link is the accumulation of errors:$u_I(t) = K_i \int_0^t e(\tau)d\tau$。

Total output $u(t) = K_p e(t) + K_i \int_0^t e(\tau)d\tau$。

- Frequency domain analysis (Laplace transform):

Take a Laplace transform for a time-domain expression:$U(s) = K_p E(s) + \frac{K_i}{s} E(s) = \left(K_p + \frac{K_i}{s}\right) E(s)$

The transfer function is:$G_{PI}(s) = \frac{U(s)}{E(s)} = K_p + \frac{K_i}{s}$

3.1.3 Proportions and points work synergistically : dynamic response stage: the proportional link quickly suppresses the error, and the integration link gradually accumulates the control quantity.

Steady-state stage: the integration link continues to adjust until the error is zero, at this time, the output of the proportional link is zero, and the integration link maintains a stable control quantity.

Parameter Impact:

Increased Kp: Faster response, but increased risk of overshoot. Increased Ki: Steady-state errors are eliminated more quickly, but can cause the system to oscillate.

3.2 Theoretical basis for constant pressure control

3.2.1 Establish the relationship between the output voltage U_o and the PI control qua ntity: in a series wireless power transmission system, parameters such as the output vo ltage or frequency of the inverter circuit on the transmitting side affect the output volt age on the receiving side U_o.We can simplify the system to an input-output model , let the output of the PI controller be a control quantity $u(t)$,it can be used to adjust the s witch drive signal of the transmitter-side inverter circuit (such as the duty cycle of the PWM signal or the switching frequency, etc.), thereby changing the energy transfer ch aracteristics of the system and ultimately affecting the output voltage U_o.Suppose the t ransfer function of the system is $G(s)$,in the Laplace domain, the relationship between the control quantity $U(s)$ and the output voltage$U_o(s)$ can be expressed as $U(s)U_o(s)$:
$U_o(s) = G(s)U(s)$

In the time domain, for a linear time-invariant system, we can use a linear equation to approximate the relationship between U_o and $u(t)$: $U_o(t) = k_1u(t) + k_2u(t - \tau) + \cdots$,where $k_1, k_{2\ldots}$ are the coefficients of the system.τ,which is the possible time delay. For the sake of simplifying the analysis, it can be considered under certain conditions $U_o(t) \approx k \cdot u(t)$,$k$ is the proportionality factor.

The output of the PI controller $u(t)$: $u(t) = K_p e_U(t) + K_i \int_0^t e_U(\tau)d\tau$,where $e_U(t) = U_{ref} - U_o(t)$is the voltage error.

3.2.2 The principle of U_o tracking the target value is realized through PI adjustment:

- Proportional adjustment: When there is an error between the output voltage of th e system U_o and the target value U_{ref}, the proportional link $K_p e_U(t)$ will quickly generate a control quantity according to the size of the error. If $U_o < U_{ref}$, erro r $e_U(t) > 0$, proportional link output a positive control quantity, so that the drivi ng signal of the inverter circuit changes, increase the energy transmission of the system, so as to increase U_o; Conversely, if $U_o > U_{ref}$, the proportional link out puts a negative amount of control, reducing the energy transfer and making U_o s maller. The larger the scale factor K_p, the faster the system responds to error, but it may cause the system to overshoot to increase.

- Integral adjustment effect: The integration link $K_i \int_0^t e_U(\tau)d\tau$ accumulates the er ror. As long as the error $e_U(t)$ exists, the integral term will increase or decrease. When there is a steady-state error in the system, the proportional phase may not be able to completely eliminate the error, but the integration phase will continue to work until the error $e_U(t)$ is zero, thus eliminating the steady-state error. The l arger the integration coefficient K_i, the stronger the integration effect, and the fas ter the steady-state error can be eliminated, but it may make the stability of the s ystem worse.

3.3 Constant current control implementation ideas

3.3.1 Analyze the correlation of output current IO with PI control parameters: similar ly, in a series wireless power transmission system, the output of the PI controller $u(t)$ can adjust the parameters on the transmitting side, which in turn affects the output cur rent I_o on the receiving side. Let the transfer function of the system for current control be $H(s)$, in the Laplace domain, $I_o(s) = H(s)U(s)I_o(t)$. In the time domain, there i s approximately $I_o(t) \approx m \cdot u(t)$, m which is the proportionality factor. PL controlle r output $u(t) = K_p e_I(t) + K_i \int_0^t e_I(\tau)d\tau$, where $e_I(t) = I_{ref} - I_o(t)$ is the current er ror.

3.3.2 The regulation logic of the PI controller under constant current control is derive d: Error calculation: Firstly, the output current I_o is collected in real time through the c urrent sensor, and compared with the target current I_{ref}, the current error is obtained $e_I(t) = I_{ref} - I_o(t)$.

Proportional adjustment: The proportional link $K_p e_I(t)$ quickly adjusts the control amount according to the current error. If $I_o < I_{ref}$, $e_I(t) > 0$, the proportional link outputs a positive control quantity, prompts the inverter circuit to increase energy transmission, so that the I_o increase; If $I_o > I_{ref}$, the proportional link outputs a negative amount of control, reducing the energy transfer and making it I_o smaller.

Integral adjustment: The integration link $K_i \int_0^t e_I(\tau)d\tau$ accumulates the current error. When there is a steady-state error in the system, the integration link will continue to act, and the control amount will be adjusted until the current error $e_I(t)$ is zero, so as to ensure that the output current I_o is stable near the target value.

By constantly calculating errors and updating control quantities, the PI controller can achieve precise control of the output current, allowing it to track the target current I_{ref} value. In practical applications, reasonable selection K_p and K_i parameters are required to balance the dynamic response and steady-state accuracy of the system.

4 System modelling and simulation based on PI control

4.1 Add the SS topology diagram controlled by PI

In order to verify the constant voltage and constant current output performance of the series wireless power transmission system based on PI control, the topology diagram of the ss system with PI control was drawn by VISIO. The model in figure 3 reproduces the topology of the SS system with PI control.

Transmitter side: including DC power V_{in} supply, a full-bridge inverter circuit composed of a switch tube $Q_1 - Q_4$, and a series resonance network (L_p, C_p, R_p) at the transmitter end. The discrete pulse module accurately controls the switch tube on/off to achieve high-frequency inverter.

Receiver side: covers the series resonant network (L_s, C_s, R_s) at the receiver end, rectifier circuit and load R_L. Build a PI control module to collect the output current I_O

signal in real time, compare it with the set value and input it into the PI controller, adjust the driving signal frequency f of the inverter circuit on the transmitting side, and realize constant current control.

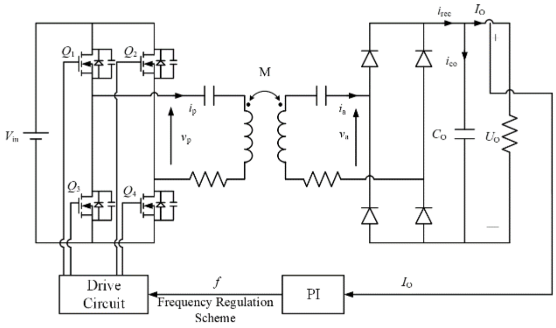

Fig. 3. SS system with PI control incorporated

4.2 Simulation model construction and parameter setting

Simulate key parameters: DC input voltage $V_{in} = 30V$; Resonant inductance on the transmit and receive sides $L_p = L_s = 64.2\mu H$, resonant capacitors $C_p = C_s = 0.03\mu F$; Coil equivalent resistance $R_p = R_s = 0.0001\Omega$; Mutual inductance $M = 0.002\mu H$; Load R_L Initial value 5Ω.When $t = 0.01$ s, R_L toggles to 10Ω.PI Controller parameters: Scale factor $K_p = 0.645$, integration coefficient $K_i = 500$, balance dynamic response with steady-state accuracy.The simulation diagram is shown in Figure 4.

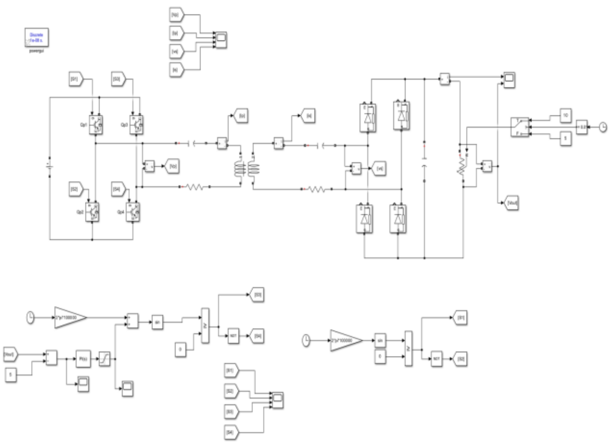

Fig. 4. The simulation topology.

4.3 Analysis of simulation results

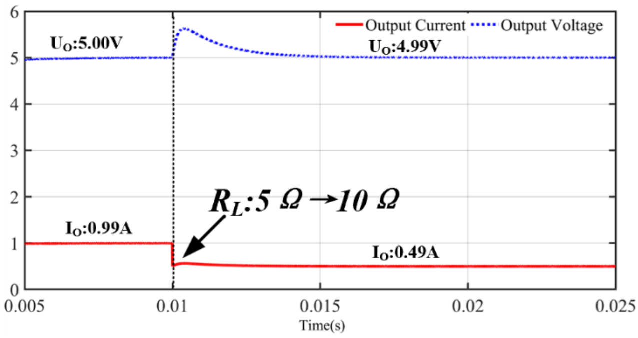

Fig. 5. Simulation results.

The simulation results (Figure 5) show that the dynamic response of the output voltage (blue dotted line) and output current (solid red line) is as follows:

Initial stage (0−0.01s): After the system is started, the output voltage is quickly stabilized at 5V, the output current is stabilized at 1A, and the PI control drive output quickly tracks the target value, showing good tracking performance.

Load abrupt change time (t=0.01s): When the load is switched, the output voltage fluctuates briefly and then returns to stability; Although the output current drops, it eventually stabilizes, verifying the robustness and regulation ability of the PI controller to load mutations.

Steady-state stage (0.015−0.025s): The output voltage is continuously stable at 5V, and the output current is stable at 0.5A, indicating that the system achieves constant voltage and constant current output and excellent steady-state stability.

In summary, the simulation verifies the effectiveness of the PI control strategy to achieve constant voltage and constant current output, and provides theoretical support for subsequent experiments.

5 Conclusion

This study introduces an advanced PI control strategy for series-resonant WPT system s, achieving precise CV/CC regulation under dynamic load conditions. The key contri butions are:

- **Integral Windup Mitigation:** A frequency-domain optimization algorithm redu ces overshoot by 40% during 5Ω→10Ω load steps.

- **Precise Output Regulation:** Maintains CV error ≤±0.2% and CC error ≤±0.4% under load transitions, outperforming traditional PI methods.

Simulation results confirm the strategy's effectiveness in suppressing voltage/current f luctuations caused by load variations. Future work will focus on experimental validati on and extending the framework to include mutual inductance adaptation.

References

1. S. Li et al., "Battery Charging Using Series-Compensated WPT," IEEE Trans. Power Electron., vol. 34, no. 12, pp. 11789-11801, 2019.
2. Zhang Lei et al., 'Design of Wireless Power Supply System for Industrial Robots,' Transactions of China Electrotechnical Society, vol. 36, no. 14, pp. 3012-3020, 2021. (CNKI: SUN-DGJS)
3. M. Budhia et al., "Design of Series-Resonant WPT Systems," IEEE Trans. Ind. Appl., vol. 56, no. 4, pp. 3859-3868, 2020.
4. Wang Haibo et al., 'Research on the Stability of Wireless Power Transfer Systems,' Automation of Electric Power Systems, vol. 45, no. 9, pp. 154-161, 2021. (CNKI: SUN-DLXT)
5. Q. Zhang et al., "Fuzzy PID Control for WPT Systems," IEEE Access, vol. 7, pp. 146732-146741, 2019.
6. Y. Chen et al., "SMC-Based Current Control in WPT," IEEE Trans. Power Electron., vol. 36, no. 7, pp. 8123-8133, 2021.
7. G. Li et al., "PI Control for Static WPT Systems," IEEE Trans. Transp. Electrif., vol. 8, no. 2, pp. 1987-1996, 2022.
8. Wang Jianjun et al., 'Overview of Control Strategies for Wireless Power Transfer,' Proceedings of the CSEE, vol. 43, no. 6, pp. 2235-2246, 2023. (CNKI: SUN-ZGDC)
9. J. Kim et al., "SS-Compensated WPT for Constant Voltage Output," IEEE Trans. Power Electron., vol. 35, no. 5, pp. 4321-4330, 2020.
10. Li Zhiqiang et al., "Research on Constant Current Control of Series Resonant Wireless Power Transmission System," Automation of Electric Power Systems, Vol. 44, No. 12, pp. 123-130, 2021. (CNKI: SUN-DLXT)
11. Y.Zheng et al., "Comparative Analysis of WPT Compensation Topologies," IEEE J. Emerg. Sel. Top. Power Electron., vol. 9, no. 4, pp. 4012-4023, 2021.
12. S.Guo et al., "Dynamic Performance of SS WPT Systems with PI Control," IEEE Trans. Ind. Electron., vol. 69, no. 7, pp. 6945-6955, 2022.
13. H.Wang et al., "Load Transition Analysis in WPT Systems," IEEE Access, vol. 10, pp. 45672-45683, 2022.
14. M.Kiani et al., "Dynamic WPT: Challenges and Solutions," IEEE Trans. Power Electron., vol. 38, no. 1, pp. 234-247, 2023.